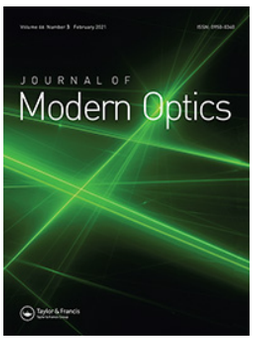

Journal of Modern Optics

ISSN: (Print) (Online) Journal homepage: https://www.tandfonline.com/loi/tmop20

Numerical study of carrier reservoir semiconductor optical amplifier-based all-optical XOR logic gate

Amer Kotb, Kyriakos E. Zoiros & Wei Li

To cite this article: Amer Kotb, Kyriakos E. Zoiros & Wei Li (2021) Numerical study of carrier reservoir semiconductor optical amplifier-based all-optical XOR logic gate, Journal of Modern Optics, 68:3, 161-168, DOI: 10.1080/09500340.2021.1885760

To link to this article: https://doi.org/10.1080/09500340.2021.1885760

Published online: 16 Feb 2021.

JOURNAL OF MODERN OPTICS
2021, VOL. 68, NO. 3, 161–168
https://doi.org/10.1080/09500340.2021.1885760

Taylor & Francis
Taylor & Francis Group

Numerical study of carrier reservoir semiconductor optical amplifier-based all-optical XOR logic gate

Amer Kotb [a,b], Kyriakos E. Zoiros[c] and Wei Li [a]

[a]GPL, State Key Laboratory of Applied Optics, Changchun Institute of Optics, Fine Mechanics, and Physics, Chinese Academy of Sciences, Changchun, People's Republic of China; [b]Department of Physics, Faculty of Science, University of Fayoum, Fayoum, Egypt; [c]Lightwave Communications Research Group, Department of Electrical and Computer Engineering, School of Engineering, Democritus University of Thrace, Xanthi, Greece

ABSTRACT

The long carrier lifetime of the semiconductor optical amplifier (SOA) limits its operation speed and exploitation as ultrafast nonlinear switching element. Therefore, an alternative SOA with a faster carrier lifetime is desired for high speed photonic applications. In this paper, we employ the carrier reservoir SOA (CR-SOA) for the first time to demonstrate through simulations the feasibility of all-optical exclusive-OR (XOR) logic gate at 100 Gb/s. For this purpose, a pair of CR-SOAs are incorporated in a Mach-Zehnder Interferometer. The variation of the quality factor (QF) against the key operating parameters is examined for both CR-SOAs- and conventional SOAs-based XOR gate at 100 Gb/s, including the effect of amplified spontaneous emission. The results show that not only higher but also acceptable QF is obtained at 100 Gb/s only when using CR-SOAscompared to conventional bulk SOAs, i.e. QF = 18.5 versus 3.3, respectively.

ARTICLE HISTORY
Received 4 January 2021
Accepted 29 January 2021

KEYWORDS
All-optical XOR logic gate; Carrier reservoir semiconductor optical amplifier; Mach–Zehnder interferometer

Introduction

The information rates of optical networks have not stopped increasing subject to the insatiable bandwidth demand and the emergence of new broadband applications [1]. In order to cope with this situation and make the most of the high capacity offered by fiber-based infrastructure, optical signal processing (OSP) has been proposed as an efficient technological approach to handle information exclusively utilizing light and thus without the practical complications of optoelectrical conversions [2,3]. The implementation of OSP critically relies on the availability of ultrafast all-optical logic gates. In particular, the exclusive-OR (XOR) gate is indispensable for realizing several fundamental and system-oriented tasks in the optical domain, such as address comparison [4], label swapping [5], pseudorandom binary sequence generation [6], encryption and decryption [7], and parity and checking [8]. For this reason, various optical technologies have been employed to execute all-optically this Boolean logic, such as highly nonlinear fibres [9], silicon waveguides [10], dielectric-loaded waveguides [11], periodically poled lithium niobate waveguides [12], photonic crystals [13], and semiconductor optical amplifiers (SOAs) [14,15]. In particular, SOAs have received extensive attention as nonlinear elements owing to their distinctive characteristics, such as strong nonlinearity, small footprint, wide bandwidth, low power consumption, and potential for integration [16]. However, conventional SOAs suffer from the long carrier lifetime of the order of hundreds of picoseconds [17], which inevitably makes difficult the straightforward extension of their operation speed beyond 100 Gb/s [17]. Therefore, it would be desirable to have an active device exhibiting the attractive features of ordinary SOAs but without their limited response. Carrier reservoir SOAs (CR-SOAs) have been proposed as one such alternative, but so far their use has been limited to classical signal amplification [18]. Therefore, in this paper, we exploit CR-SOAs' comparative advantage over conventional SOAs with regard to faster response to execute for the first time the XOR logic at 100 Gb/s. To this aim, we investigate and assess the switching potential of CR-SOAs when incorporated in the Mach–Zehnder Interferometer (MZI) by comparison against that of standard SOAs. For this purpose, we account for the effect of critical operating parameters on the quality factor (QF) in the presence of (CR-) SOA

CONTACT Amer Kotb amer@ciomp.ac.cn GPL, State Key Laboratory of Applied Optics, Changchun Institute of Optics, Fine Mechanics, and Physics, Chinese Academy of Sciences, Changchun 130033, People's Republic of China; Department of Physics, Faculty of Science, University of Fayoum, Fayoum 63514, Egypt; Wei Li weili1@ciomp.ac.cn GPL, State Key Laboratory of Applied Optics, Changchun Institute of Optics, Fine Mechanics, and Physics, Chinese Academy of Sciences, Changchun 130033, People's Republic of China

amplified spontaneous emissions (ASE) noise for more realistic results. The theoretical outcomes confirm the feasibility of employing CR-SOAs as nonlinear elements for designing and realizing all-optical logic gates capable of keeping pace with the data rates trends in modern optical networks and systems.

Principle of operation

CR-SOA

Figure 1 shows the CR-SOA band diagram, where a carrier reservoir (CR) region is placed close to the active region (AR) [16]. The injection current into the CR-SOA moves the carriers to fill the available states in both AR and CR. In the presence of an input optical power, the carriers of the AR are depleted by the stimulated emission process. These depletion-uncopied states are directly filled by the carriers from the CR in an ultrashort transition time of 0.5–5 ps. Consequently, the CR accumulates sufficient carriers to act as a reservoir of supplied carriers leading to the acceleration of the device operating speed.

XOR logic

The schematic diagram and truth table of the XOR logic gate using CR-SOAs-based MZI are shown in Figure 2.

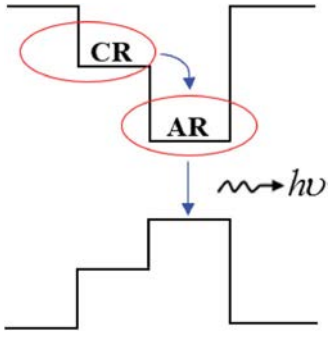

Figure 1. Band diagram of CR-SOA.

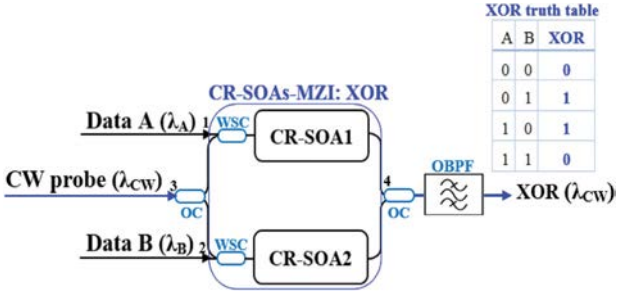

Figure 2. Schematic diagram and truth table of XOR logic gate using CR-SOAs-MZI. OC: 3 dB optical coupler. WSC: wavelength-selective coupler. OBPF: optical bandpass filter.

More specifically, two identical CR-SOAs are placed in the two arms of the MZI. To realize the XOR operation between data A and B two such signals at wavelengths λ_A and λ_B are injected via wavelength-selective couplers (WSCs) into CR-SOA1 from port 1 and into CR-SOA2 from port 2, respectively. A continuous-wave (CW) beam acting as the probe is launched at the setup from port 3 and is equally split by a 3 dB optical coupler (OC) into two parts which enter CR-SOA1 and CR-SOA2, respectively. These CW beams interact with the pulses of streams A and B, which modulate the gain and phase of the CW beams via cross-gain modulation and cross-phase modulation processes. When these CW beams recombine at the OC located at port 4, they produce different outputs depending on the driving conditions. Thus when both A and B are '0' or '1', the CW output beams experience the same gain and phase while propagating the MZI arms and so interfere destructively at port 4, thus resulting in '0' output. However, when A is '0' and B is '1' or vice versa, the CW beams undergo different gain and phase modulation to constructively interfere at port 4, thereby resulting in '1' output. In this manner, the optical circuit produces a '1' at its output if only if one of the inputs A or B is '1'. This operation corresponds to the XOR logic whose outcome imprinted on the exiting CW beam at wavelength λ_{CW} is selected by an optical bandpass filter (OBPF).

Simulation

In the conducted numerical simulation, data inputs A and B between which the XOR function is executed are assumed to carry return-to-zero pulses of Gaussian-shaped profile having energy E_0, full-wave half maximum (FWHM) pulse width τ_{FWHM}, and bit period T, i.e. [14,15]:

$$P_{A,B}(t) \equiv P_{in}(t) = \sum_{n=1}^{N} a_{n(A,B)} \frac{2\sqrt{\ln[2]}\,E_0}{\sqrt{\pi}\,\tau_{FWHM}} exp\left[-\frac{4\ln[2](t-nT)^2}{\tau_{FWHM}^2}\right] \quad (1)$$

where $\alpha_{n(A,B)}$ represents the n-th pulse along a pseudo-random binary sequence (PRBS) of length $N = 2^7$-1, i.e. $\alpha_{n(A,B)}$ = '1' or '0'. Since data signal A of power P_A is combined with half of the CW beam and injected into the MZI upper arm, while data signal B of power P_B is combined with the other half of the CW beam and injected into the MZI lower arm, the input powers in the scheme shown in Figure 1 are expressed as:

$$P_{in,\,CR-SOA_1}(t) = P_A(t) + 0.5\,P_{CW} \quad (2)$$

$$P_{in,\,CR-SOA_2}(t) = P_B(t) + 0.5\,P_{CW}. \quad (3)$$

where the coefficient '0.5' takes into account the coupling of the CW beam of power P_{CW} into the middle arm of the (CR-)SOAs-MZI.

Taking into account the nonlinear intraband effects of carrier heating (CH) and spectral hole burning (SHB), the CR-SOA time-dependent gain is described by the following set of coupled differential equations [16,18]:

$$\frac{dh_{AR}(t)}{dt} = \frac{h_{CR}(t)-h_{AR}(t)}{\tau_t(1+\eta)} + \frac{\eta h_0}{\tau_c(1+\eta)} - \frac{h_{AR}(t)}{\tau_c} - (exp\,[h_{AR}(t)+h_{CH}(t) + h_{SHB}(t)] - 1)\,\frac{P_{in}(t)}{E_{sat}} \quad (4)$$

$$\frac{dh_{CR}(t)}{dt} = -\frac{\eta(h_{CR}(t)-h_{AR}(t)}{\tau_t(1+\eta)} + \frac{h_0-h_{CR}(t)}{\tau_c(1+\eta)} - \frac{h_{CR}(t)}{\tau_c} \quad (5)$$

$$\frac{dh_{CH}(t)}{dt} = -\frac{h_{CH}(t)}{\tau_{CH}} - \frac{\varepsilon_{CH}}{\tau_{CH}} - (\exp\,[h_{AR}(t) + h_{CH}(t)+h_{SHB}(t)] - 1)\,P_{in}(t) \quad (6)$$

$$\frac{dh_{SHB}(t)}{dt} = -\frac{h_{SHB}(t)}{\tau_{SHB}} - \frac{\varepsilon_{SHB}}{\tau_{SHB}} - (\exp\,[h_{AR}\,(t) + h_{CH}(t)+h_{SHB}(t)] - 1)\,P_{in}(t) - \frac{dh_{AR}(t)}{dt} - \frac{dh_{CH}(t)}{dt} \quad (7)$$

where functions 'h' denote the CR-SOA gain integrated over its length for the carrier recombination between AR (h_{AR}) and CR (h_{CR}), CH (h_{CH}), and SHB (h_{SHB}).
τ_t is the transition time from the CR layer to the AR layer and
τ_c is the recombination lifetime in both AR and CR. η is the population inversion factor defined as $\eta = N_{AR}/N_{CR}$, where N_{AR} and N_{CR} are the carrier densities in AR and CR, respectively. $h_0 = \ln[G_0]$, where the unsaturated power gain is defined as $G_0 = \acute{E}\acute{S}\Gamma(I\tau_c/eV - N_{tr})$ [16], where $\acute{E}\acute{S}$ is the differential gain, Γ is the confinement factor, I is the injection current, e is the electron charge, V is the volume of the AR, N_{tr} is the transparency carrier density, and L is the length of the AR. E_{sat} is the saturation energy defined by $E_{sat} = P_{sat}\,\tau_c = wd\hbar\omega_0/\acute{E}\acute{S}\Gamma$ [16], where P_{sat} is the saturation power, w & d are the width and thickness of the AR, respectively, $\hbar$ is the normalized Planck's constant (i.e. $h/2\pi$), and ω_0 is the input signal central frequency. τ_{CH} and τ_{SHB} are the CH and SHB temperature relaxation rates, respectively. ϵ_{CH} and ϵ_{SHB} are the CH and SHB nonlinear gain suppression factors, respectively.

The above model, which was originally proposed for the case of CR-SOA direct signal amplification [18], is valid since its principal theoretical prediction, namely that CR-SOAs have a faster response than regular SOAs, verifies the same evidence obtained experimentally and reported in [19]. This fact allows us to proceed and explore, for the first time, the proven and demonstrated ultrafast potential of CR-SOAs in the MZI for all-optical signal processing applications, such as all-optical logic realization. The favourable correlation between theory and experiment enhances our confidence that our numerical calculations will be valid too, thus rendering the extracted results and drawn conclusions useful towards enabling the real implementation of CR-SOA-based logic gates.

Then the total integrated gain of each CR-SOA is given by [16,20]:

$$G_{CR-SOA_i}(t) = exp[h_{AR}(t) + h_{CH}(t) + h_{SHB}(t)],\quad i = 1,\ 2 \quad (8)$$

The phase change induced on the CW beams in each CR-SOA is expressed by [16,20]:

$$\Phi_{CR-SOA_i}(t) = -0.5(\alpha\, h_{AR}(t) + \alpha_{CH}\, h_{CH}(t)),\ i = 1,2 \quad (9)$$

where α is the traditional linewidth enhancement factor, known as α-factor, α_{CH} is the CH linewidth enhancement factor, and the contribution of SHB is null, i.e. $\alpha_{SHB} = 0$ [14,15].

At port 4, the CW beams extracted from the two CR-SOAs interfere to form the XOR output whose power is described by the following interferometric expression [16]:

$$P_{XOR}(t) = 0.25\,P_{CW}\,\left(G_{CR-SOA_1}(t) + G_{CR-SOA_2}(t) - 2\sqrt{G_{CR-SOA_1}(t)\,G_{CR-SOA_2}(t)}\,cos\,[\Phi_{CR-SOA_1}(t) - \Phi_{CR-SOA_2}(t)]\right) \quad (10)$$

where $G_{CR-SOA1,2}(t)$ and $\Phi_{CR-SOA1,2}(t)$ are the gains and phase responses of CR-SOA1 and CR-SOA2, respectively.

Results and discussion

The performance of the XOR gate using both CR-SOAs- and conventional SOAs-assisted MZI is evaluated against the quality factor (QF). The QF is characterized by its high sensitivity in estimating the quality of the output signals. This metric is defined as the difference between the average peak powers of 1's and 0's at the XOR gate output divided by the sum of the corresponding standard deviations, i.e. $QF = (P_1 - P_0)\ /\ (\sigma_1 + \sigma_0)$ [14,15]. A minimum value of QF = 6 is necessary to ensure acceptable

Table 1. Default parameters [14–27].

Symbol	Definition	Value	Unit
E_0	Pulse energy	0.1	pJ
τ_{FWHM}	Pulse width	1	ps
T	Bit period	10	ps
N	PRBS length	127	–
λ_A	Wavelength of data A	1545	nm
λ_B	Wavelength of data B	1550	nm
λ_{CW}	Wavelength of CW	1556	nm
P_A	Power of data A	1.2	mW
P_B	Power of data B	1.2	mW
P_{CW}	Power of CW	0.27	mW
I	Injection current	300	mA
P_{sat}	Saturation power	30	mW
τ_c	Carrier lifetime	300	ps
τ_t	Transition lifetime from CR to AR	5	ps
η	Population inversion factor	0.3	–
α	α-factor	4	–
α_{CH}	CH linewidth enhancement factor	1	
α_{SHB}	SHB linewidth enhancement factor	0	ns
ϵ_{CH}	CH nonlinear gain suppression factor	0.1	W^{-1}
ϵ_{SHB}	SHB nonlinear gain suppression factor	0.1	W^{-1}
τ_{CH}	Temperature relaxation rate	0.3	ps
τ_{SHB}	Carrier-carrier scattering rate	0.1	ps
Γ	Optical confinement factor	0.4	–
$\acute{E}\acute{S}$	Differential gain	1×10^{-20}	m^2
N_{tr}	Transparency carrier density	1×10^{24}	m^{-3}
L	Length of AR	500	μm
d	Thickness of AR	0.3	μm
w	Width of AR	3	μm
G_0	Unsaturated power gain	30	dB
N_{SP}	Spontaneous emission factor	2	–
υ	Optical frequency	193.55	THz
B_0	Optical bandwidth	2	nm
$\hbar$	Reduced Planck's constant	1.05×10^{-34}	J.s

performance, or equivalently to keep the related bit-error-rate below 10^{-9} [21]. The following results were obtained by solving the above rate equations for both CR-SOA and conventional SOA using Adam's numerical method in Wolfram Mathematica®. The default parameters cited in Table 1 [14–27] are used for both schemes for a fair comparison.

Figure 3 depicts the comparison of the gain dynamics for the CR-SOA and standard SOA within the frame of the XOR operation at 100 Gb/s. From this figure, it can be seen that the gain response of the normal SOA suffers from a strong-pattern effect, which manifests as pronounced amplitude fluctuations (Figure 3(a)). Figure 3(b) shows instead that the impaired gain recovery process of the ordinary SOA is considerably improved for the CR-SOA since the latter provides a faster gain response enabled by the ultrafast transition due to the existence of the CR layer. This fact renders the CR-SOA a more suitable nonlinear device for supporting higher speed Boolean operations with pattern-free performance, as it is the case for a stand-alone CR-SOA [28], compared to an ordinary SOA whose response is limited by its slower dynamics.

Figures 4 and 5 illustrate the numerical results for the XOR gate between data A and B at 100 Gb/s using

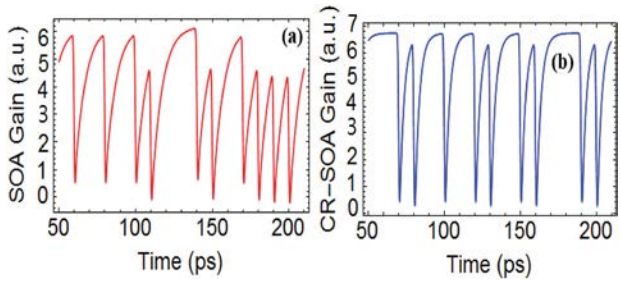

Figure 3. Gain response for (a) conventional SOA and (b) CR-SOA at 100 Gb/s.

CR-SOAs- and conventional SOAs-assisted MZI, respectively. Although the XOR logic is correctly executed for both devices, yet the profile of the logical outcome when using the conventional SOAs strongly deviates from that when using the CR-SOAs. In fact, pulses suffer from intense peak amplitude fluctuations and the corresponding eye diagram is strongly distorted in the first case. On the contrary, pulses become quite uniform and the eye diagram is clear and open in the second case. These differences are reflected on the attained QF, which is much higher, i.e. 18.5, with CR-SOAs than 3.3 with normal SOAs. This means that while the all-optical XOR logic gate cannot be operated with acceptable QF at 100 Gb/s using conventional SOAs-MZI, yet this is more than possible using CR-SOAs-MZI. The primary reason for achieving acceptable and higher QF when using the CR-SOAs-based scheme is the ultrafast transition from the occupied CR layer to the AR layer.

Both the transition lifetime from CR to AR (τ_t) and the population inversion factor (η) play an important role in the CR-SOAs gain recovery. Therefore, it is important to study the influence of these parameters on the performance of the XOR gate. Figure 6 shows the variation of the QF against τ_t and η using the CR-SOAs-based MZI. More specifically, Figure 6(a) shows that a shorter τ_t results in faster gain recovery and hence higher QF. This is practically possible as τ_t has been measured to lie in the range of $\sim$ 0.5–5 ps in GaAs [16]. On the other hand, η quantifies the carrier density in the CR and AR, i.e. $\eta = N_{AR}/N_{CR}$, and hence the amount of carriers available for ultrafast gain recovery. Thus for smaller η, which corresponds to a higher CR population, the gain recovery is faster and as a natural result, the QF is increased, as shown in Figure 6(b).

The ASE noise being present in both types of considered SOAs can affect negatively the quality of the XOR gate outcome, so its effect should be taken into account. The influence of ASE noise is calculated by $P_{ASE} = N_{SP}\ (G_0 - 1)\ 2\pi\hbar\upsilon B_0$ [14,15], where B_0 is the optical bandwidth at frequency υ and N_{SP} is the spontaneous emission factor being ideally equal to 2. The ASE

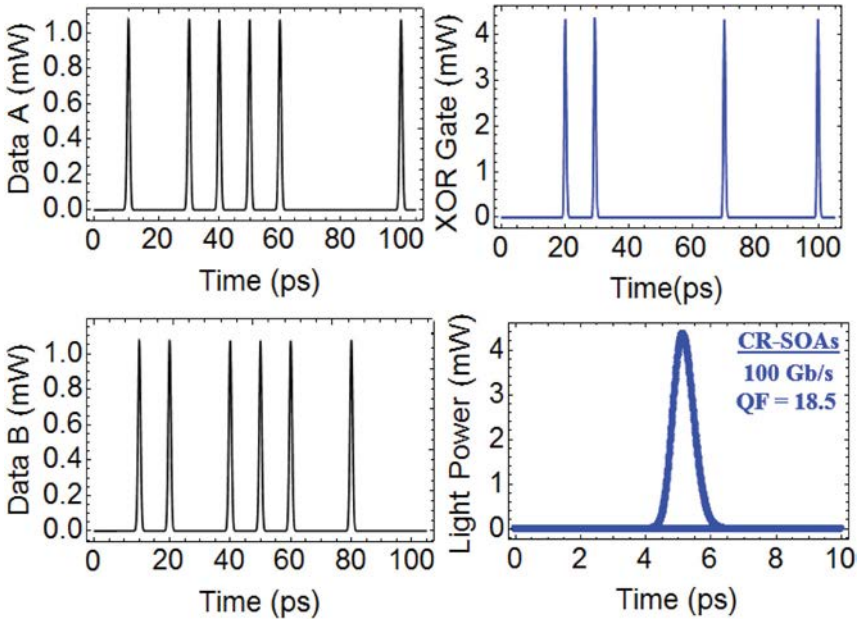

Figure 4. Results of XOR logic gate between data A and B using CR-SOAs-MZI achieving 18.5 QF at 100 Gb/s.

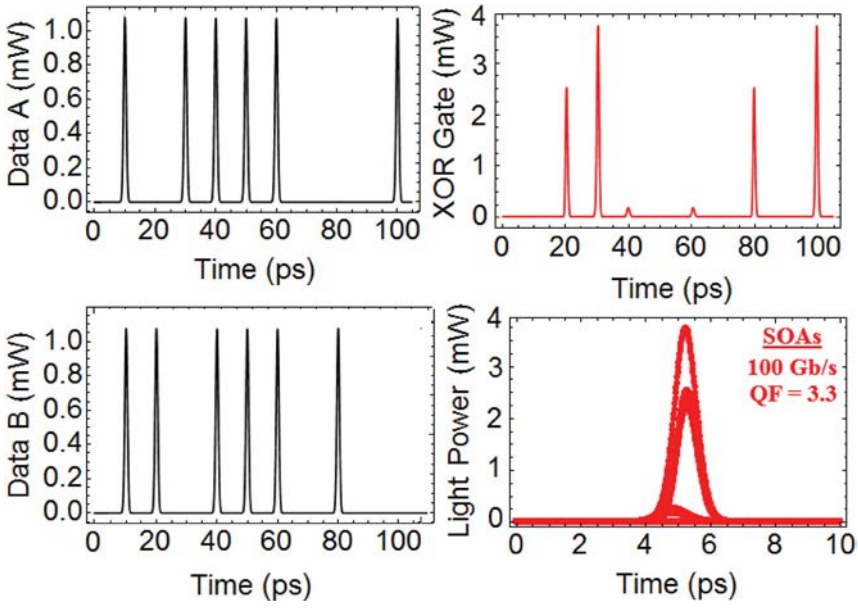

Figure 5. Results of XOR logic gate between data A and B using SOAs-MZI achieving 3.3 QF at 100 Gb/s.

power is added to that of the logical outcome obtained for the four logical combinations of the data inputs. This is a common approach that has previously been adopted in other works studying the logic performance of MZI switches incorporating novel SOA-based devices against the quality factor (see for instance [*29*]), and implies that ASE does not affect the CR-SOAs gain saturation. This is a valid approach [*30*], since the input data pulses saturate strongly both SOAs, as it can be verified from the gain response variation depicted in Figure 3. Besides, the SOA-MZI performance critically depends on ASE when long SOAs ($> 1500\,\mu m$) are used [*31*], which however is not our case. Figure 7(a) shows that the QF is degraded with increasing ASE power for both CR-SOAs- and SOAs-based XOR gate at 100 Gb/s. This happens because the ASE power is numerically added to the XOR output power, which in turn enhances the mean peak power of '0' bits and accordingly leads, by definition of the QF, to a decrease of the latter. Nevertheless, it is also noticed that the CR-SOAs succeeds in achieving an acceptable QF even at higher values of the ASE power. Although the ASE power can impair the QF, yet its level

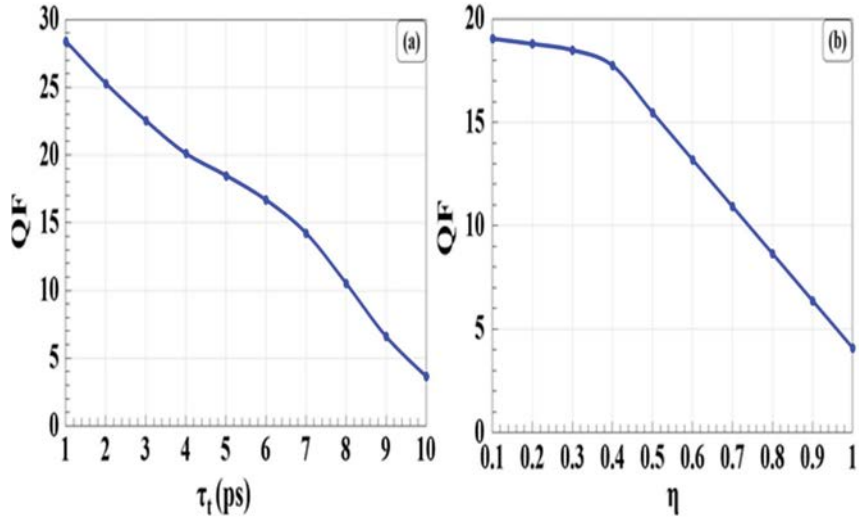

Figure 6. QF of XOR logic gate at 100 Gb/s using CR-SOAs versus (a) transition time from CR to AR (τt) and (b) population inversion factor (η).

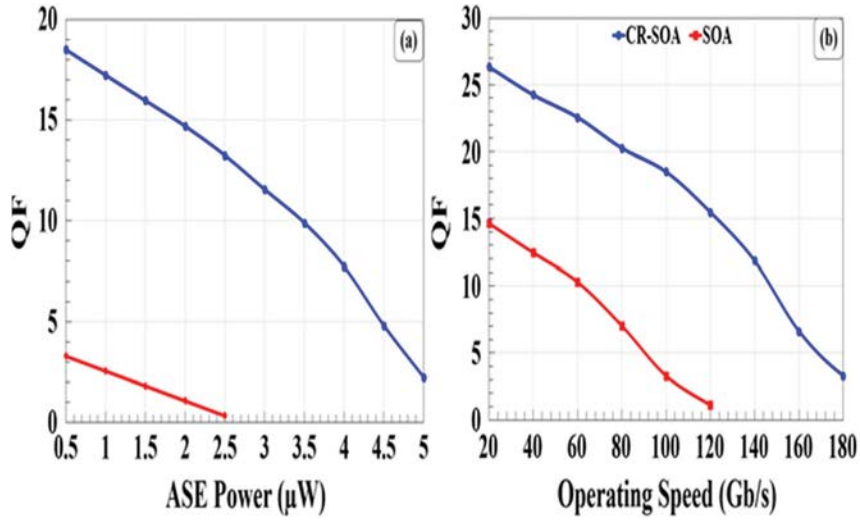

Figure 7. QF of XOR logic gate using CR-SOAs and conventional SOAs versus (a) amplified spontaneous emission (ASE) power and (b) operating speed.

is negligible compared to that of the logical outcome obtained for both CR-SOA (Figure 4) and conventional SOA (Figure 5). For this reason, no raise of the baseline is discernible in either Figure 4 or Figure 5. On the other hand, an important issue concerning the upgradability of the XOR gate is up to which speed the CR-SOAs, under the specified operating conditions, can maintain the QF acceptable. Figure 7(b) addresses this issue as it depicts the change in the QF with the operating speed for both CR-SOAs- and SOAs-based XOR gate. From this figure, we notice that the CR-SOA allows the scheme to operate with acceptable performance, i.e. QF = 6.63, up to 160 Gb/s, in line with modern trends, while this is not possible with the conventional SOA. Physically this happens because the inherently slower response of

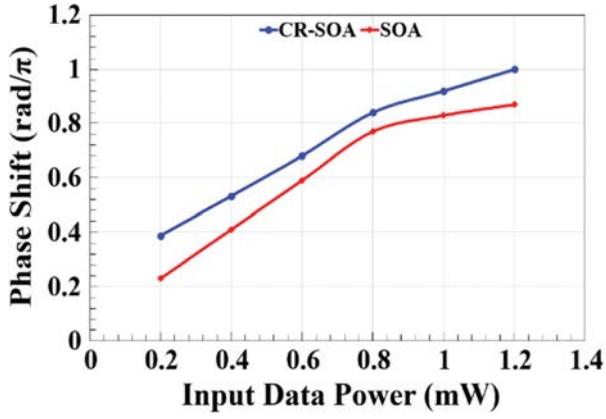

Figure 8. Induced phase shift versus input data power for CR-SOA and normal SOA at 100 Gb/s.

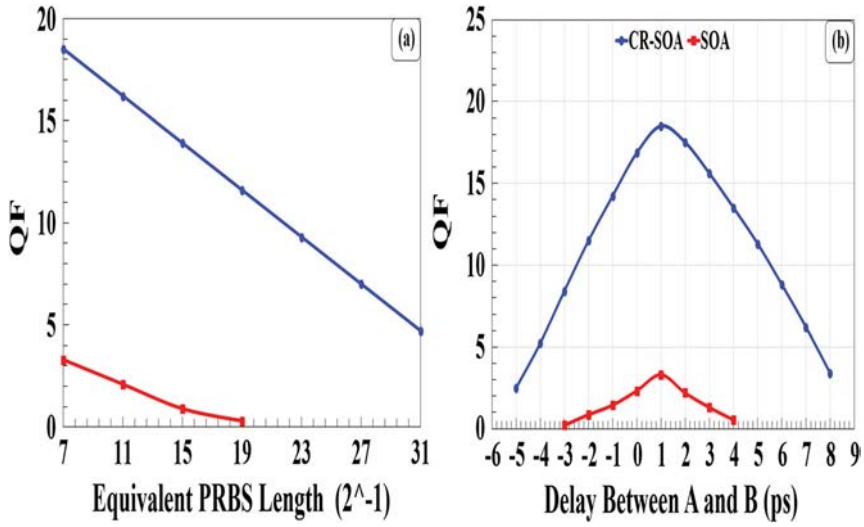

Figure 9. QF of XOR logic gate using CR-SOAs and conventional SOAs versus (a) equivalent PRBS length and (b) delay between signals A and B at 100 Gb/s.

the conventional SOA constitutes a fundamental limiting factor, while placing a CR layer close to the AR one in the CR-SOA allows to efficiently circumvent this obstacle.

The extent of the phase shift induced in CR-SOAs and conventional SOAs by the input data at 100 Gb/s is plotted in Figure 8 against the power of these excitation signals. It can be observed that the phase shift induced when using conventional SOAs is smaller than when using CR-SOAs for the same input power. At an input power level of 1.2 mW, the phase shift within the standard SOAs cannot reach the amount of π, which is required for full interferometric switching [*32*] while this is achieved when using CR-SOAs due to the faster gain and phase response.

Figure 9(a) shows the QF versus the equivalent PRBS length [*33*] for the all-optical XOR logic gate at 100 Gb/s using both CR-SOAs- and conventional SOAs-based MZI. Using a higher-order PRBS, it can be seen that the CR-SOAs-MZI retains its acceptable and high performance even for a rather long standardized PRBS, meaning that it is quite insensitive to strong pattern effects, since the latter scale with the PRBS length [*34*], owing to the faster and uniform CR-SOAs response, while this is not possible with the regular SOA-MZI. Similar results are obtained when the data inputs are not perfectly synchronized, as it may be the practical case in a real all-optical signal processing node [*33*]. In fact, Figure 9(b) shows that the CR-SOA-based scheme is quite tolerant to such an offset up to 70% of the repetition period, while this is not possible at all with the conventional SOA. Figure 9(b) also shows that shorter delays between A and B increase the QF, which becomes maximum at 1 ps, i.e. at the FWHM employed in this study.

Conclusions

In this study, we examined the feasibility of implementing the all-optical XOR gate using CR-SOAs compared to conventional SOAs in a MZI at an operating speed of 100 Gb/s. Due to the faster gain recovery of CR-SOAs, the latter allow to achieve better results with acceptable performance than their counterparts, even in the presence of high ASE noise and up to 160 Gb/s. Therefore, CR-SOAs can form a viable technological alternative from which XOR logic and the various applications that rely on it can benefit from a practical and essential perspective.

Acknowledgments

Amer Kotb thanks the CAS President's International Fellowship Initiative (PIFI) (grant number 2019FYT0002) and the Talented Young Scientist Program (TYSP) in China for supporting this work.

Disclosure statement

No potential conflict of interest was reported by the author(s).

Funding

Amer Kotb thanks the CASPresident's International Fellowship Initiative (PIFI) (grant number 2019FYT0002) and the Talented Young Scientist Program (TYSP) in China for supporting this work.

ORCID

Amer Kotb http://orcid.org/0000-0002-3776-822X
Wei Li http://orcid.org/0000-0002-2227-9431

References

[1] Semrau D, Xu T, Shevchenko NA, et al. Achievable information rates estimates in optically amplified transmission systems using nonlinearity compensation and probabilistic shaping. Opt Lett. **2017**;41:121–124.

[2] Saruwatari M. All-optical signal processing for terabit/second optical transmission. IEEE J Sel Top Quantum Electron. **2000**;6:1363–1374.

[3] Willner AE, Khaleghi S, Chitgarha MR, et al. All-optical signal processing. J Lightwave Technol. **2014**;32:660–680.

[4] Hamilton SA, Robinson BS. 40-Gb/s all-optical packet synchronization and address comparison for OTDM networks. IEEE Photon Technol Lett. **2002**;14:209–211.

[5] Martínez JM, Liu Y, Clavero R, et al. All-optical processing based on a logic XOR gate and a flip-flop memory for packet-switched networks. IEEE Photon Technol Lett. **2007**;19:1316–1318.

[6] Zoiros KE, Houbavlis T, Kalyvas M. Ultra-high-speed all-optical shift registers and their applications in OTDM networks. Opt Quantum Electron. **2004**;36:1005–1053.

[7] Jung YJ, Son CW, Lee S, et al. Demonstration of 10 Gbps, all-optical encryption and decryption system utilizing SOA XOR logic gates. Opt Quantum Electron. **2008**;40:425–430.

[8] Nielsen M, Petersen M, Nord M, et al. Compact all-optical parity calculator based on a single all-active Mach-Zehnder interferometer with all-SOA amplified feedback. Proc OFC TuQ2; 2003.

[9] Sun K, Qiu J, Rochette M, et al. All-optical logic gates (XOR, AND, and OR) based on cross-phase modulation in a highly nonlinear fiber. 2009 35th European Conference on Optical Communication, Vienna; 2009.

[10] Gao S, Wang X, Xie Y, et al. Reconfigurable dual-channel all-optical logic gate in a silicon waveguide using polarization encoding. Opt Lett. **2015**;40:1448–1451.

[11] Yao C, Kotb A, Wang B, et al. All-optical logic gates using dielectric-loaded waveguides with quasi-rhombus metasurfaces. Opt Lett. **2020**;45:3769–3772.

[12] Wang J, Sun Q, Sun J. Ultrafast all-optical logic AND gate for CSRZ signals using periodically poled lithium niobate. J Opt Soc Am B. **2009**;26:951–958.

[13] He L, Zhang WX, Zhang XD. Topological all-optical logic gates based on two-dimensional photonic crystals. Opt Express. **2019**;27:25841–25859.

[14] Kotb A, Zoiros KE, Guo C. All-optical XOR, NOR, and NAND logic functions with parallel semiconductor optical amplifier-based Mach-Zehnder interferometer modules. Opt Laser Technol. **2018**;108:426–433.

[15] Kotb A, Guo C. All-optical multifunctional AND, NOR, and XNOR logic gates using semiconductor optical amplifiers. Phys Scr. **2020**;95:085506.

[16] Dutta NK, Wang Q. Semiconductor optical amplifiers. 2nd ed Singapore: World Scientific Publishing Company; 2013.

[17] Mørk J, Nielsen ML, Berg TW. The dynamics of semiconductor optical amplifiers: Modeling and applications. Opt Photon News. **2003**;14:42–48.

[18] Sun H, Wang Q, Dong H, et al. Gain dynamics and saturation property of a semiconductor optical amplifier with a carrier reservoir. IEEE Photon Technol Lett. **2006**;18:196–198.

[19] Eisenstein G, Tucker RS, Wiesenfeld JM, et al. Gain recovery time of traveling-wave semiconductor optical amplifiers. Appl Phys Lett. **1989**;54:454–456.

[20] Kotb A, Guo C. 120 Gb/s all-optical NAND logic gate using reflective semiconductor optical amplifiers. J Mod Opt. **2020**;67:1138–1144.

[21] Zhang X, Dutta NK. Effects of two-photon absorption on all-optical logic operation based on quantum-dot semiconductor optical amplifiers. J Mod Opt. **2017**;65:166–173.

[22] Kotb A, Guo C. Theoretical demonstration of 250 Gb/s ultrafast all-optical memory using Mach-Zehnder interferometers with quantum-dot semiconductor optical amplifiers. IEEE J Sel Top Quantum Electron. **2021**;27:7700307.

[23] Kotb A. Simulation of high-quality-factor all-optical logic gates based on quantum-dot semiconductor optical amplifier at 1 Tb/s. Optik. **2016**;126:320–325.

[24] Ezra YB, Lembrikov BI, Haridim M. Ultrafast all-optical processor based on quantum-dot semiconductor optical amplifiers. IEEE J Quantum Electron. **2008**;17:34–41.

[25] Rostami A, Nejad HB, Qartavol RM, et al. Tb/s optical logic gates based on quantum-dot semiconductor optical amplifiers. IEEE J Quantum Electron. **2010**;46:354–360.

[26] Sun H, Wang Q, Dong H, et al. XOR performance of a quantum dot semiconductor optical amplifier based Mach-Zehnder interferometer. Opt Express. **2005**;13:1892–1899.

[27] Wang Q, Zhu G, Chen H, et al. Study of all-optical XOR using Mach-Zehnder interferometer and differential scheme. IEEE J Quantum Electron. **2004**;40:703–710.

[28] Wan SM, Tsang HK, Su YS, et al. Inhibiting pattern-effects in semiconductor optical amplifier using carrier reservoir in an asymmetrical multiple quantum well structure. Proc. OFC OWI85, 2006.

[29] Gayen DK, Chattopadhyay T. Designing of optimized all-optical half adder circuit using single quantum-dot semiconductor optical amplifier assisted Mach-Zehnder interferometer. J Lightwave Technol. **2013**;31:2029–2035.

[30] Bischoff S, Buxens A, Fischer S, et al. Comparison of all-optical co- and counter-propagating high-speed signal processing in SOA-based Mach–Zehnder interferometers. Opt Quantum Electron. **2001**;33:907–926.

[31] Schares L, Schubert C, Schmidt C, et al. Phase dynamics of semiconductor optical amplifiers at 10 to 40 GHz. IEEE J Quantum Electron. **2003**;39:1394–1408.

[32] Papadopoulos G, Zoiros KE. On the design of semiconductor optical amplifier-assisted Sagnac interferometer with full data dual output switching capability. Opt Laser Technol. **2011**;43:697–710.

[33] Siarkos T, Zoiros KE. Performance of single semiconductor optical amplifier–based ultrafast nonlinear interferometer with clock-control signals timing deviation in dual rail-switching mode. Opt Eng. **2009**;48:085004.

[34] Xu J, Zhang X, Mørk J. Investigation of patterning effects in ultrafast SOA-based optical switches. J Quantum Electron. **2010**;46:87–94.